Available online at www.sciencedirect.com
ScienceDirect
Ceramics International 35 (2009) 373–380
CERAMICS INTERNATIONAL
www.elsevier.com/locate/ceramint

Improvement of corrosion resistance of spinel-bonded castables to converter slag

S. Mukhopadhyay [a,*], T.K. Pal [b], P.K. DasPoddar [a]

[a] Department of Chemical Technology, Calcutta University, 92 A.P.C. Road, Kolkata 700009, India
[b] Metallurgical Engineering Department, Jadavpur University, Kolkata 700032, India

Received 10 June 2007; received in revised form 13 September 2007; accepted 12 November 2007
Available online 23 December 2007

Abstract

Limited chemisorbed hydroxyl groups around the crystalline entity of gel-route spinel powder helped to create nanopores in castable to resist slag penetration. The retained nanodimensional spinel in fired castable firmly connected hibonite and corundum grains, developed several interfaces after initial stage of densification, and arrested the detrimental ions of slag. XRD, scanning electron microscope (SEM) with atomic force microscope (AFM) studies of the nanostructured spinel-bonded castables corroborated their better properties than similar kind bonded with preformed spinel. The performance of spinel with 90% alumina and the conventional in situ spinel-bonded castables were satisfactory whereas the coprecipitated spinel was not commendable.

Keywords: Spinel; Refractory castable; Slag corrosion; Nanostructured ceramics

1. Introduction

Steel-making processes are associated with highly corrosive slags and aggressive reactions giving rise to erosive conditions. At par with the advancement of steel-making processes, an unprecedented demand has also been imposed on quality, maintenance and capability of specially tailored refractories. Development of monolithic castables brought a paradigm shift for refractory industry and over the last 20 years there has been a great change in unit consumption of refractories. The application of alumina–spinel and alumina–magnesia castables in ladles is well known. Their characteristics, comparative performances and selection criterion are also well documented [1–3]. There has been a profound interest for the production of ceramic nanopowders via chemical routes for various technological applications [4,5]. In our previous report, it has been outlined that such reactive ultrafine spinel powders in castable might cope with the hostile atmosphere of steel ladles. This paper extends the comparative study of several spinel-bonded castables.

It includes the possibility of embedding in situ nanocrystalline spinel particles in a dense, bulk castable after primary stage of heating and their structural modification after further consolidation [6]. It has already been outlined that the modified sol–gel route has the ability to assemble these nanostructures in a micro- or meso-scale structure in a controlled manner. It was postulated there that OH-ligands can be carefully designed around spinel particles by redox condensation; thus the growth of nanoparticles could be protected by a thin layer of (OH) groups, which act as reducing agent during the synthesis of spinel nanoparticles.

It investigates the feasibility of retention of such spinel particles in a castable after initial heat treatment by atomic force microscope (AFM) supplemented with XRD studies. It also includes the comparative performance of alumina-rich (R-type) spinel-bonded alumina-based castable with that nanocrystalline counterpart, especially in terms of slag resistance and its interpretation by scanning electron micrographs [7–10]. In this context, in situ Al_2O_3–MgO with another preformed (P-type) spinel–alumina castable and coprecipitated spinel-bonded castable [10–12] have also been taken into

* Corresponding author. Tel.: +91 33 2350 8386; fax: +91 33 2351 9755.
E-mail address: msunanda_cct@yahoo.co.in (S. Mukhopadhyay).

0272-8842/$34.00
doi:10.1016/j.ceramint.2007.11.008

consideration to complete this investigation with a reasonable conclusion.

2. Experimental

The spinel hydrogel, as mentioned in our earlier work, put some adverse effects when used in castable batch beyond a certain amount. Due to this, the semidried gel precursors (G and C) were activated by 'soft' mechanochemical treatment [13] and optimally calcined at 900 °C. Modified in situ spinel additives were thus prepared after passing them through 200-mesh BS (below 75 μm) sieve. These fine materials [11] were considered to be the important constituents of the respective matrices of the castable batches, which also remained the same as reported in our work [11]. Two commercial preformed spinel powders (P and R) were collected from the market [11], to incorporate into the new castable batch. All such powders had been utilized one at a time separately in equal amount (i.e. 8.0 wt%). Light and pure MgO fine (code M [11]) was also added to that batch to prepare in situ spinel-bonded high alumina (i.e. $MgO–Al_2O_3$) castable.

The procedure for castable preparation (named RN, GN, PN, MN and CN in accordance with the additives used) included dry and wet mixing of the batch, both done for 30 min to enhance the consistency of the mix. The mass was then cast in moulds and tamped within a particular time period. The material being self-flow type, no vibration was applied from outside. Curing in humid condition (for 24 h), air drying (24 h) and oven drying (at 110 °C for 3 days) were strictly followed for all the samples. Finally they were heat treated (at 5–8 °C/min) to 900, 1200, 1500 and 1600 °C, with a holding period of 2 h in each case as reported in our previous articles. It is worthwhile to mention that the performance of RN type castable has not been reported in our last articles [10]. In this paper, therefore, the quality of RN castable has been examined distinctively in comparison with others especially in terms of slag resistance and microstructural analysis.

To corroborate the nanodimensional characteristics of the sol–gel spinel additive and the respective castable, it was very much essential for this work to investigate and compare the interaction of different spinel-forming materials with the matrix part of the castable. As appeared in our articles [10], finer fraction below 75 μm had been treated as the matrix part of the castable batch. In this regard a simulated matrix composition of the spinel-free castable, same as that given in our previous paper [11], was formulated first. The matrix compositions of different castables were then prepared accordingly, by incorporating the respective contribution (at par with 8.0 wt%) of each type spinel. All of them were cast at the identical condition as discussed above and fired at 1500 °C/2 h. These samples were selected for scanning electron microscope (SEM) studies because as stated afterwards, that particular temperature was vital to attest both spalling and slag resistances. A proportionate amount of fine (below 75 μm) basic slag (Table 1), collected from VSL (India) was gently rammed with the matrix part of the GN castable and fired at 1500 °C/2 h. This slag-treated GN matrix was also subjected to

Table 1
Composition of basic converter slag

Constituents	Amount (wt%)
CaO	47.6
SiO_2	15.0
MgO	10.6
FeO	20.5
Al_2O_3	1.3
MnO	2.0

SEM with energy-dispersive spectral (EDS) analyses to examine the effect of nanodimensional spinel in the matrix, especially to explore whether and how it improves the slag-resistance behaviour. G and P additives being closer in composition, the AFM topography study too, of the matrix part

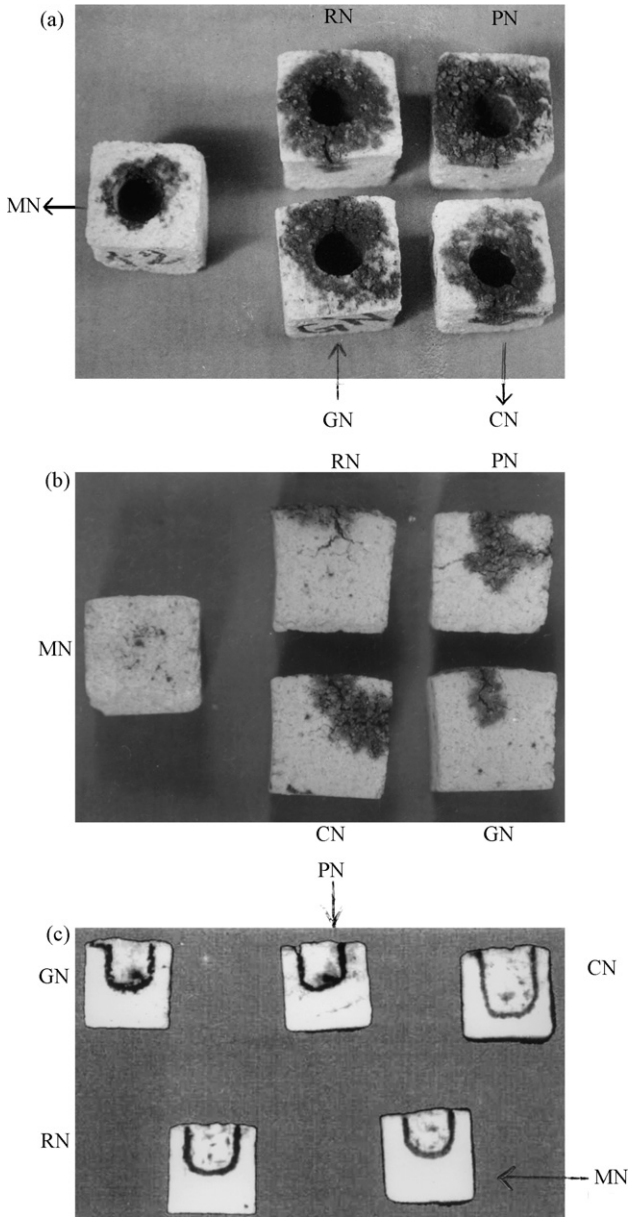

Fig. 1. Photographs of slag-corroded castables (five types) after 1500 °C/2 h: (a) top view, (b) front view and (c) cut-section view.

of GN and PN castables, was done in this connection to distinguish between their surface morphologies after precalcination. It was a digital contact mode instrument (Model: NANOSCOPE IV) with a Si_3N_4 oscillating tip.

For microstructural evaluation of the fired GN, MN, CN, PN and RN castables, SEM with EDS studies were conducted with the instruments JEOL JSM 5200 and Hitachi S-2300 models. To study the slag resistance of RN-, GN-, PN-, MN- and CN-type castables, the visual inspection of the cubes (top view, front view and cut section) was done minutely after severely heat-treating them (1500 °C/2 h) with the supplied slag. This was a simplified version of the laboratory slag cup or cavity test [14–16], in which both penetration and corrosion patterns were noted carefully. To emphasize the role of nanosized spinel, the slag corroded matrix part of GN castable was additionally taken into account by SEM and EDS tests, as mentioned above.

3. Results and discussion

The visual observation of corrosion effect (Fig. 1(a)–(c) of five kinds of castables by the slag (Table 1) indicates that the penetration and corrosion effects have been optimally controlled in GN castable. If all the three views of slag-corroded castables are observed, it is clear that the corrosion resistance and penetration resistance are better, respectively in MN and RN types. The performance of CN is not recommendable. Between PN and GN, both having the spinel composition with close chemistry, it is obvious that GN ranks better. This can be corroborated and more reasonably explained if we observe the AFM figures of PN and GN next to the following discussion.

Fig. 2(a)–(c) shows the XRD patterns of GN, RN and MN type of slag-corroded castables. R-type spinel, is known to dissolve indirectly in iron-containing slag [17], and such spinels can engulf more cations from the slag because of more number of cation (Mg^{2+})-vacancies in their structure. Consequently, slag viscosity increases and it is difficult to penetrate into the castable. The formation of lattice-defective spinels and entrapment of detrimental ions from slag, are clear from the XRD patterns of slag-affected GN and RN castables (Fig. 2(a) and (b)). However, as the dissolution of R-type spinel is indirect, and comparatively less slag is needed to dissolve it completely, therefore, its corrosion resistance is not so encouraging. Al_2O_3–MgO castable, on the other hand, is supposed to be the best when slag corrosion resistance is considered. MgO fines with high surface area undergo all-pervasive spinel formation above 1200 °C, which improves slag-resistance property. Other related mechanisms, in terms of

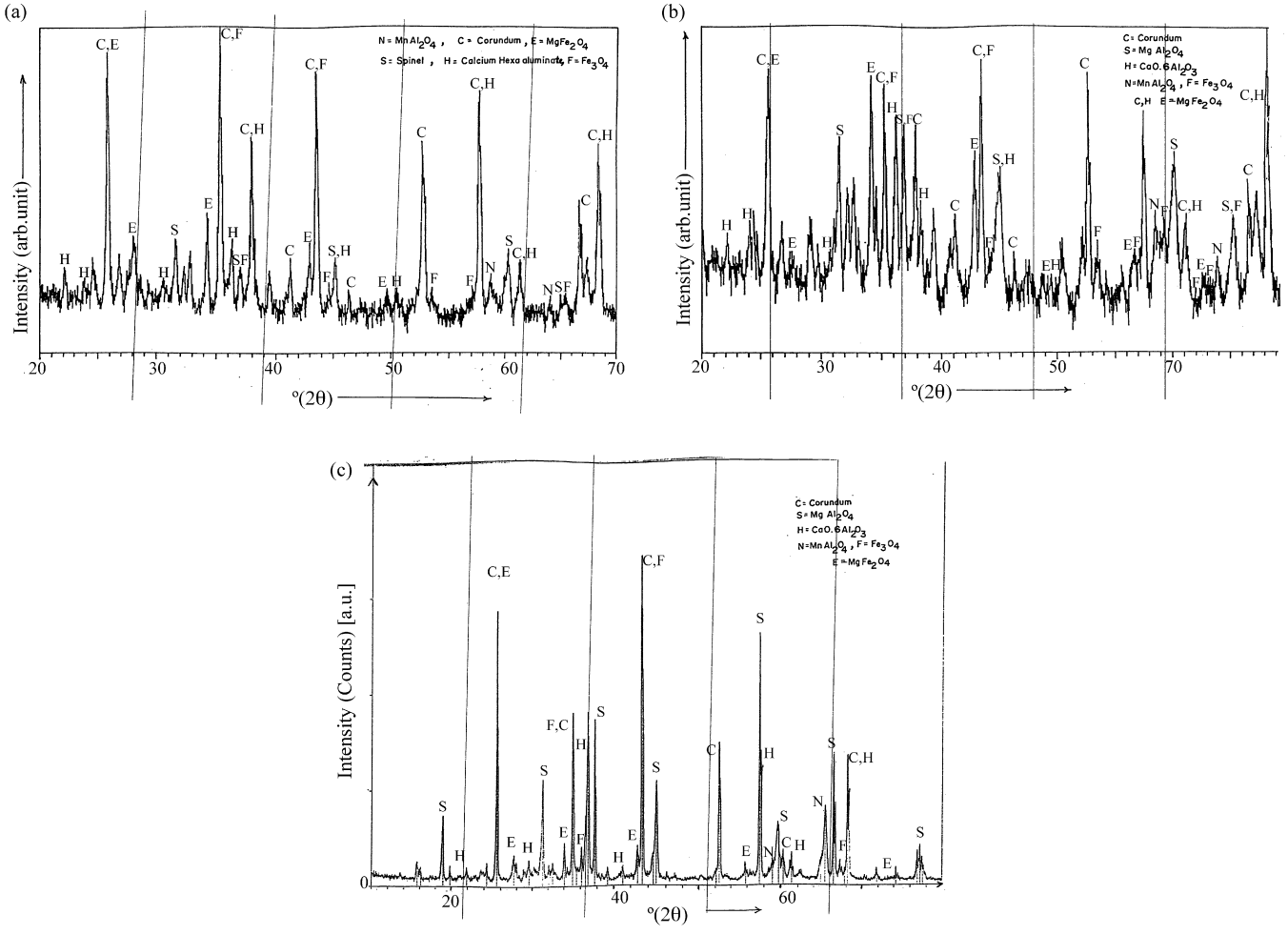

Fig. 2. XRD patterns of different types of castables after the slag corrosion test: (a) GN type, (b) RN type and (c) MN type.

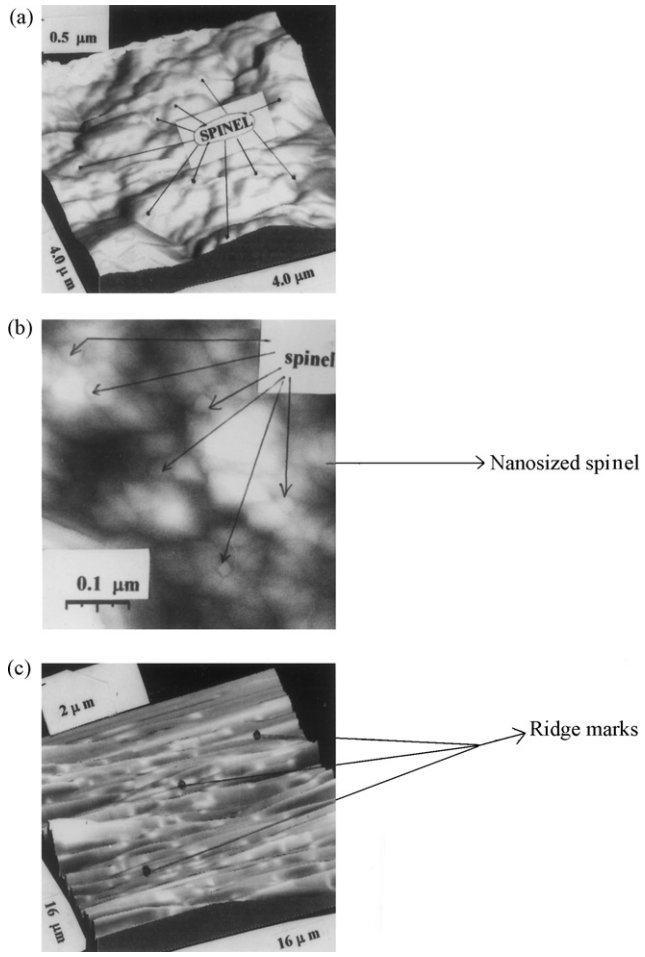

Fig. 3. AFM topographic patterns of the matrix part of (a) GN castable after 900 °C, (b) GN castable fired at 1500 °C and (c) PN castable fired at 1500 °C.

slag penetration depth (h), solid–liquid interfacial energy (G_{sl}), change in viscosity (η), precipitation of MgO, etc. had also been proposed [18]. Fig. 2(c) shows that in MN castable, an extensive amount of spinel has been generated, which might be the reason to depress slag corrosion [19], although, it exerts lower resistance to slag penetration [10]. It has been reported [20] that enstatite and albite-type compounds are also generated in such castables. In GN, unlike other two, slag resistance and penetration are optimally controlled. From the XRD report (Fig. 2(a)), it is clear that apart from C–A–S and C–A–F [S=SiO_2, F=Fe_2O_3] enriched phases, a lot of complex spinel-forming compounds with general formula [(MgFeMn)O(Al-Fe)$_2O_3$] have been generated in the matrix. Highly reactive G additive helps to generate such compound at the slag-refractory interface to render a passive-corrosion effect that slows down the corrosive agent approaching towards the substrate. CA_6 compounds are formed by the reaction between fine Al_2O_3 from matrix and CaO from slag, which also retard the slag penetration. At the same time, nanopores associated with the GN castables help to divert the slag-assisted cracks and their further invasion into the refractory. Usually there remains a fluid 'outer layer' of slag over a 'viscous' inner layer directly in contact with the refractory surface. In GN, slag might react with refractory to expose more nanostructured matrices and nanopores at the intermediate hot face. These remnant nano-interfaces of spinel must also prevent the severity of slag by altering the adherence, contact angle and wettability parameters. Secondly, although the grain-boundary phase is known to allow a relatively fast transport of the corroding agent into the material, yet such kind of internal corrosion is also capable of slowing down with time [21]. As the remnant nanostructured grains offer a huge amount of grain-boundary area, they also

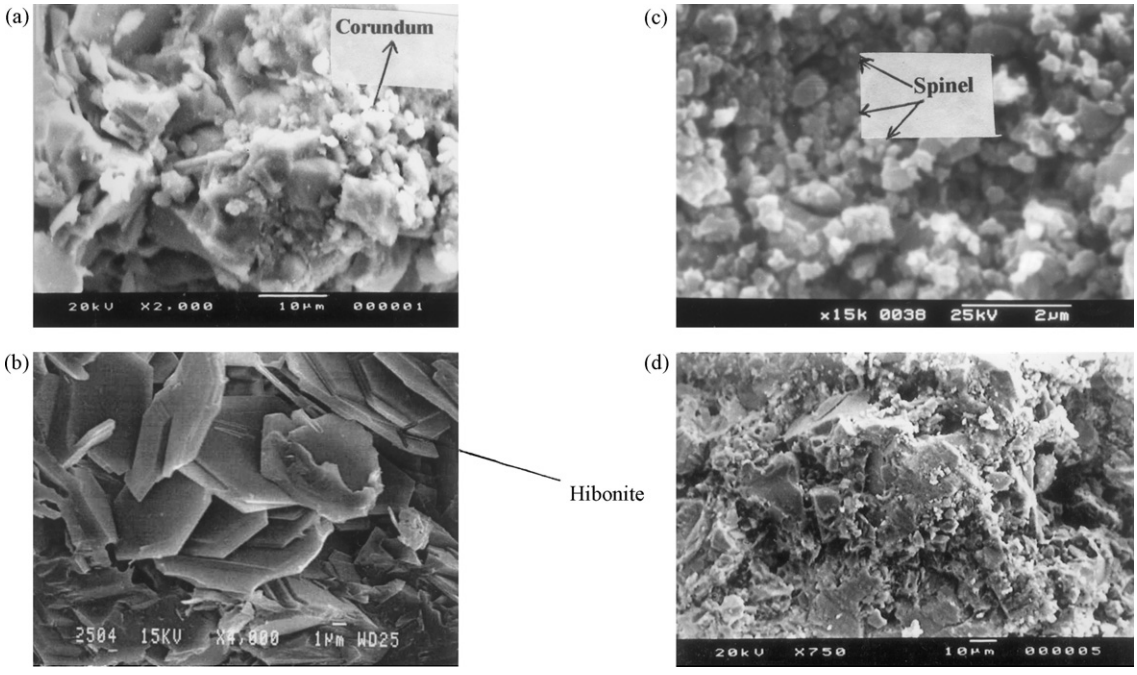

Fig. 4. Scanning electron micrographs of RN-type castable fired at 1600 °C (a and b); scanning electron micrographs of matrices of RN-type castable fired at 1500 °C (c and d).

possess some protective quality towards internal corrosion. After several heats, indeed, the nanophases of spinel dissolve in matrix to result in another desired CMAS phase which bridges the cracks. The poor performance of PN and CN towards slag corrosion had been explained elsewhere [10].

Fig. 3(a) and (b) shows, respectively the surface analysis of the matrix part of GN castable after 900 and 1500 °C. Fig. 8(c) is the similar representation of the PN matrix after heat treatment at 1500 °C. Fig. 8(a) clearly shows that the nanophase spinel is present in the castable material. With due course of heating, the (OH) caps around the nanoparticles are lost, some submicronized pores appear nearby, while the sporadic and bare nanostructured regions get trapped within the matrix. Even after first heating cycle (at 1500 °C), some nanometric regions are still observed (Fig. 3(b)) in the two-dimensional AFM image of the surface of GN matrix. Moderately uniform color intensity suggests that most of the phases are similar in nature and density. They also indicate homogeneity and smoothness of the surface as revealed by little variations in the height and phase images [22]. On the other hand, in PN castable (Fig. 3(c)), uneven surfaces clearly appear as ridge marks. Furthermore, when oscillating tip moves over the surface, streaks and elongated images appear; this might be attributed to the movement of phases when the debris are dragged along the tip. All these confirm the presence of lose particles, weak bonding and surface irregularities in PN. Oppositely due to the overwhelming evidence of rigid nanostructured matrix of GN, the slag resistance of GN stood better than PN, although the two additives G and P [10,11] have closer chemical composition.

The performance of RN, GN, PN and other two castables can be well understood if we observe the microstructures of the fired counterparts in terms of phase assemblage, pore-size distribution, grain size and orientation, texture and so on. For this reason the heat-treated castable (1600 °C) as a whole as well as the matrix part (1500 °C) of selected samples were chosen.

Figs. 4–8 show the micrographs of RN-, PN-, GN-, CN- and MN-type castables after heat treatment. The RN (Fig. 4), PN (Fig. 5) and GN (Fig. 6) show an overall morphological similarity with enough of hexagonal cardlike CA_6 phases, which is the most abundant in RN type. Those net-like phases interconnect the corundum and spinel grains to improve the performance of such castable, especially the hot strength of RN type (Fig. 4(a) and (b)). The SEM of the matrix part of fired RN-type castable (Fig. 4 (c) and (d)) also corroborates that the matrix has been enriched with CA_6 phases, might be due to extra corundum phases associated with 'R' additive. The properties of all five castables showed considerable difference as revealed from the microstructures.

The CCS of GN as outlined in our previous papers [6,10], is better than PN below 900 °C for the desirable CMAS phase with an interwoven morphology to hold the grains. Nevertheless, the CCS after 900 °C is better in PN, because the true specific gravity of G additive is almost 17% less than the presintered densified spinel [10,11]. Moreover as the fineness of G was below 75 μm and that of P was below 45 μm, thus the particle-size effect seems to contribute a role towards the

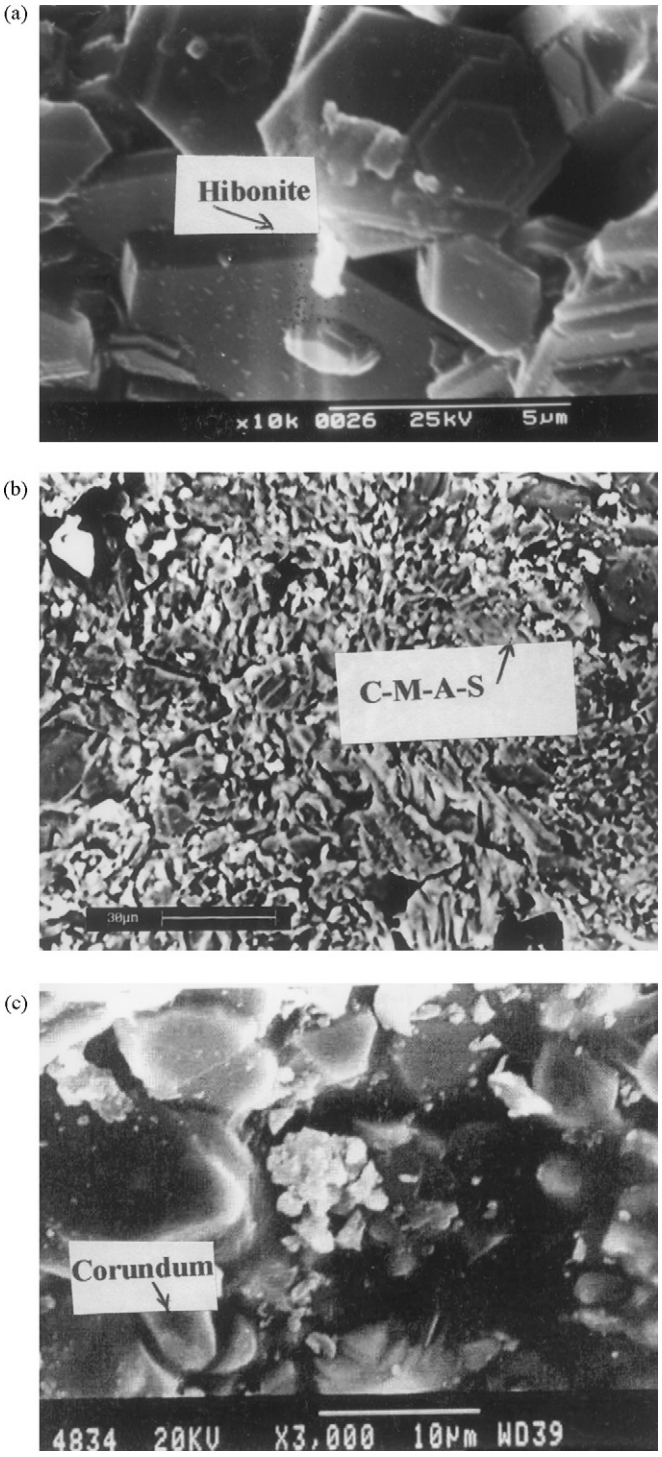

Fig. 5. Scanning electron micrographs of PN-type castable fired at 1600 °C (a and b); scanning electron micrographs of matrix of PN-type castable fired at 1500 °C (c).

strength values of castables. The porosity of GN castable is poor in comparison to PN (Fig. 5(a)–(c)) and might be due to the remnant OH-groups present in the additive that are eliminated later after thermal treatment. However, this little drop in porosity may be sacrificed if those distributed micropores can be utilized to upgrade the R.S.% of GN in comparison with PN [23]. As the density of RN is much higher

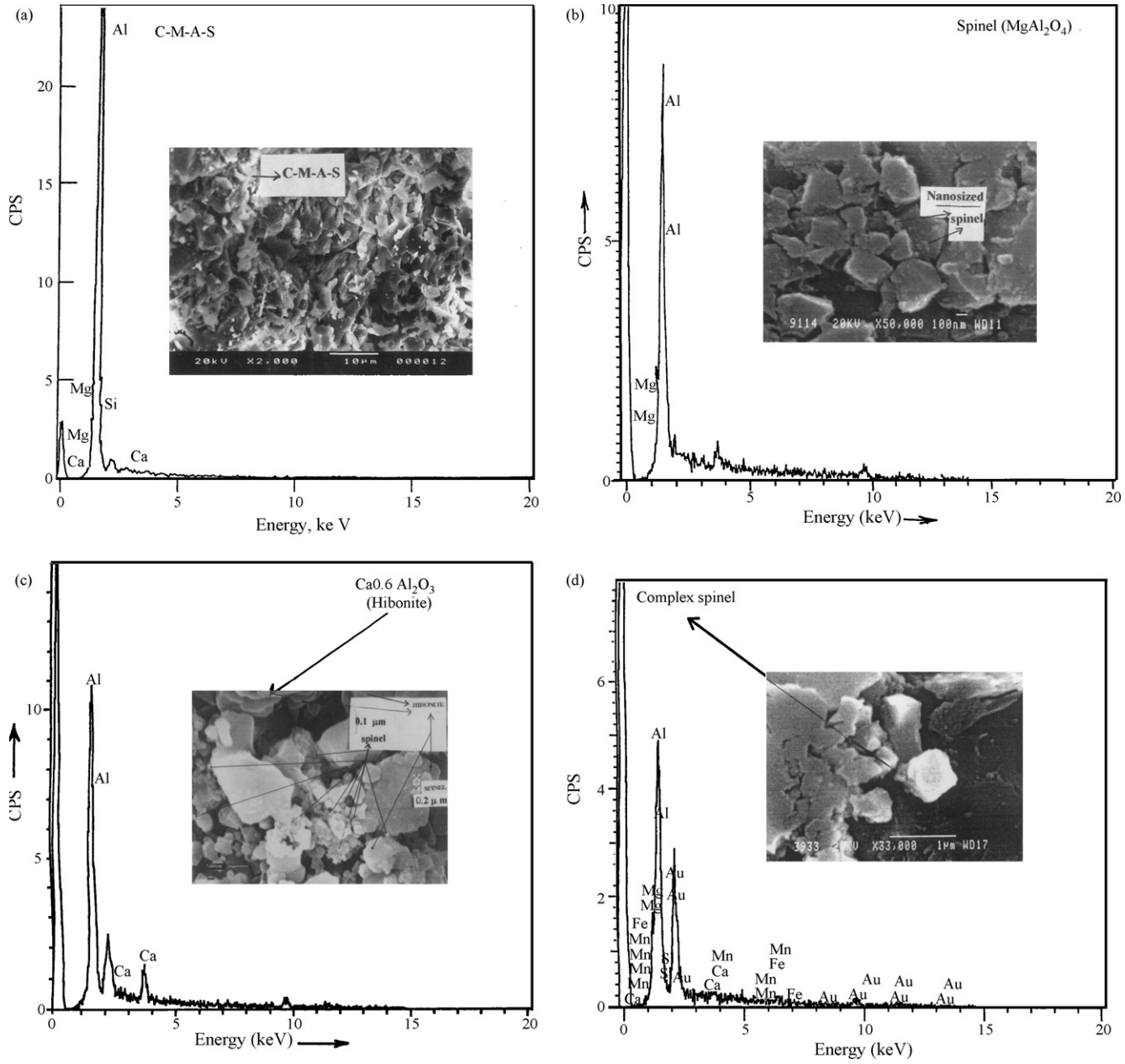

Fig. 6. Scanning electron micrographs (with EDS) of: (a) GN castable fired at 1600 °C; (b) the fractured surface of the matrix of GN castable fired at 1500 °C; (c) the matrix of GN fired at 1500 °C; (d) slag-corroded GN matrix after 1500 °C.

than PN, the spalling resistance of RN (R.S.% = 51) is inferior to the PN (56%) as expected.

Fig. 6 shows the microstructural evolution of GN castable at elevated temperature. The net-like morphology enriched with CMAS phase, as observed at 1600 °C in Fig. 6(a) is very much desirable in spinel–alumina castable. It is to some extent refractory and efficiently holds corundum and hibonite grains with the spinel phases present in the matrix. The EDS pattern in Fig. 6(a) confirms the presence of well-developed CMAS phase in castable. The presence of viscous CMAS phase must also assist to hold the cracked faces together during thermal shock and corrosion assisted crack growth to enhance the maximum work of fracture of castable matrix. It may also be suggested that the matrix-advantage-system in this castable has been developed by the high degree of 3D connectivity of hibonite and corundum grains with the reactive nanocrystallites of spinel additive. Fig. 6(b) and (c) shows the fired (1500 °C) matrix of GN refractory which again confirms the presence of well-dispersed nanophase spinel particles through the matrix. These inter- and intra-granularly distributed spinel fines might have some influence to improve the slag corrosion resistance of GN castable. Due to the distributed submicronized pores, the corrosive slags need to exert much greater impact stress to erode the refractory [15]. The nanophase spinel crystallites differing in coordination and local site symmetry from the bulk also help to efficiently engulf the unwanted ions (Fe^{2+}, Mn^{2+}) from slag. Consequently the slag composition becomes rich in silica and could not penetrate the castable.

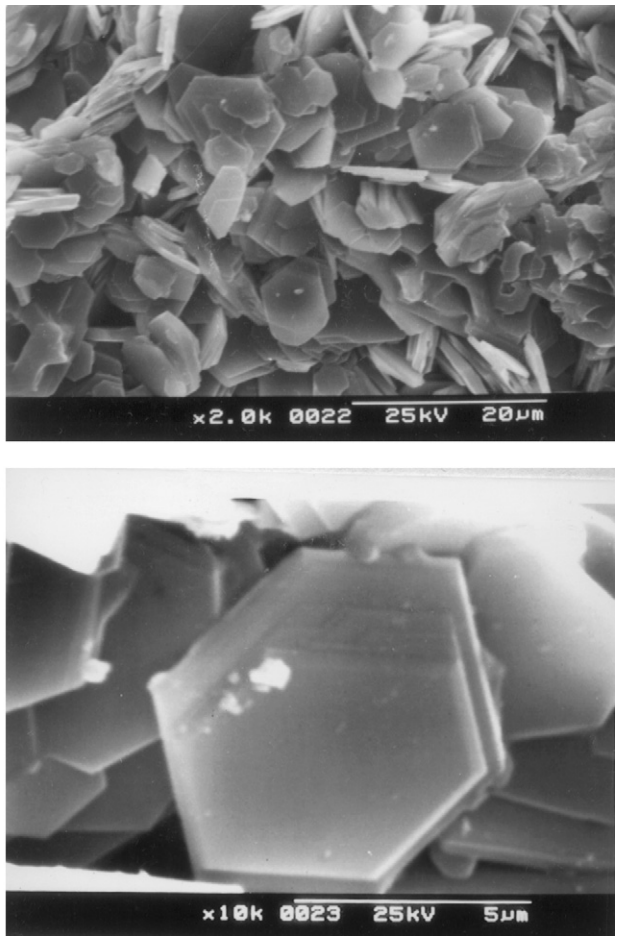

Fig. 7. (a and b) Scanning electron micrographs of CN castable fired at 1600 °C.

The agreable performance of GN-type castable becomes clearer from the other SEM and EDS figures (Fig. 6(b) and (c)) of the corresponding fired material. It reveals that some nano-fine spinel domains have been generated in matrix that is directly bonded with corundum and hibonite grains. This kind of modification of matrix by the self-assemblage of spinel crystallites is possible because of the effective sinterability of sol–gel (G) additive [24,25]. They occupied the space between medium and large grains and formed necks and bridges as found in the SEM of the fractured surface. Fig. 6(b) shows the spinel crystallites with nearly nanoscale dimensions embedded in the matrix. The retention of such phases after sintering is the additional benefit of the flexible sol–gel route, which enables tuning the pore size, surface area, composition and density of the additive. It also improved the hot strength of GN castable as observed in our previous articles.

Fig. 6(d) once more strongly supports these nanodimensional characteristics of the G-type spinel additive. The arrow-marked region in that figure is the point where EDS plot has been taken. It is evident that the slag-affected GN matrix contains those unwanted ions (Fe^{2+}, Mn^{2+}) in the complex spinel solid solution at the vicinity of a vitreous ($CaO–Al_2O_3–SiO_2$) phase. The entrapment of those detrimental ions from slag occurred might be due to the reactive nanodimensional spinels exposed throughout the matrix as observed in the AFM figure before. The high magnifications of the SEM figure, along with that of the other micrograph Fig. 6(b) and (c), firmly indicate the presence of nanopores nearby the nanostructured spinels.

The bimodal distribution of particles in 'C' additive might have hindered the densification and delayed the spinel evolution. The properties of CN, therefore, might have been degraded due to some abnormal growth of grains (Fig. 7(a) and (b)). A lot of microcracks generated after the residual hydroxyls released from the additive, also caused a serious limitation in terms of AP and CCS of the castable. However, the G additive with a precise control over its stoichiometry and due to the presence of reactive nanosized spinels in its structure might have easily formed the CMAS phase (Fig. 6) in castable and assisted densification [25].

As the formation of abnormal grains of spinel in MN matrix is extensive above 1500 °C, it is not unlikely that the CMAS phase has not been grown properly in the respective castable (Fig. 8). Theoretically 8.0 wt% fine MgO present in MN castable should give almost 28.4% spinel if the reaction is complete [26]. This reaction might have decreased the alumina content in the matrix with an inevitable weakening of MA–CA_6–Co (i.e. spinel–hibonite–corundum) linkage. At the same time the spinel forming reaction itself is known to be volume-expansive [27]. As a result, high porosity (~35%) and low CCS values already created due to the decomposition of brucite and hydrotalcite, were very much difficult to compensate later, by sintering alone. Large permeable pores already generated in MN might worsen the penetration resistance, despite the improvement of corrosion resistance by extensive in situ spinellisation.

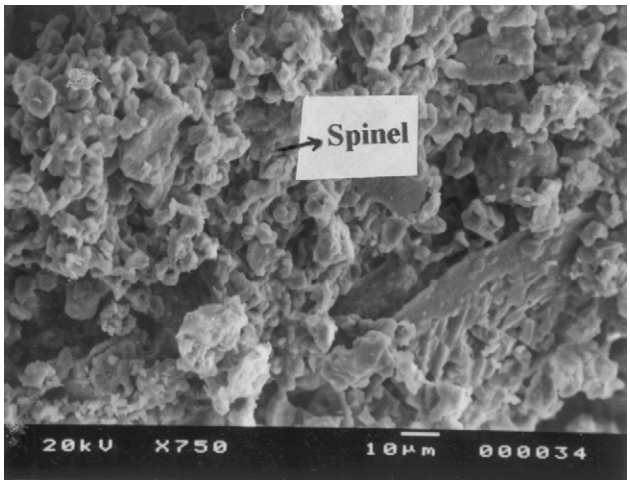

Fig. 8. Scanning electron micrograph of MN castable fired at 1600 °C.

4. Conclusions

From this laboratory scale investigation, the following conclusions may be drawn:

(1) The (OH)-induced layer gives rise to distributed nanopores in the fired castable after initial heating along with some nanostructured region trapped in the matrix. After next heating cycles, they densify the matrix and play an important role to resist slag corrosion with other improved properties. This sol–gel spinel can be taken into account for a comparison with P-type preformed spinel, if commercially produced.
(2) The preformed spinel with 90% alumina can arrest a lot of ions from converter slag due to their structural vacancies. The slag-resistance property of in situ spinel-bonded castable is also good whereas the castable bonded with coprecipitated spinel is not so encouraging.

Acknowledgement

The authors are thankful to Mr. Rahul Lodha, Research Scholar, Department of Materials Engineering (Ceramics), Vancouver, Canada, the University of British Columbia for his help extended during the preparation of this paper.

References

[1] M. Suguwara, T. Asano, The recent developments of castable technology in Japan, in: Proceedings of the 9th UNITECR-2005, November 8–11, Orlando, FL, USA, 2005.
[2] G. Ye, G. Oprea, T. Troczynski, Spinel bonded magnesia versus spinel bonded spinel castables, in: Proceedings of the 9th UNITECR-2005, November 8–11, Orlando, FL, USA, 2005.
[3] V. Bhatnagar, S. Mukhopadhyay, C. Natarajan, Development of improved quality spinel castable for steel ladle bottom, in: Proceedings of the 9th UNITECR-2005, November 8–11, Orlando, FL, USA, 2005.
[4] R.K. Pati, P. Pramanik, Low temperature chemical synthesis of nanocrystalline $MgAl_2O_4$ spinel powder, J. Am. Ceram. Soc. 83 (2000) 1822–1824.
[5] S. Takanaga, Y. Fujiwara, M. Hatta, Nano-Tech. refractories-3, development of MgO-rimmed MgO–C brick, in: Proceedings of the 9th UNITECR-2005, November 8–11, Orlando, FL, USA, 2005.
[6] (a) S. Mukhopadhyay, P.K. DasPoddar, Evolution of nanoscale microstructural features in unshaped refractories by prospective spinel ($MgAl_2O_4$) gel, Interceram. 56 (1) (2007) 25–28;
(b) S. Mukhopadhyay, P.K. DasPoddar, Evolution of nanoscale microstructural features in unshaped refractories by prospective spinel ($MgAl_2O_4$) gel, Interceram. 56 (2) (2007) 104–107.
[7] R.M. Evans, Magnesia–alumina–spinel, Am. Ceram. Soc. Bull. 72 (1993) 59–63.
[8] M.W. Vance, G.W. Kriechbaum, R.A. Henrichsen, G. Maczura, K.J. Moody, S. Munding, Influence of spinel additives on high-alumina/spinel castables, Am. Ceram. Soc. Bull. 73 (1994) 70–74.
[9] M. Kobayashi, K. Kataoka, Y. Sakamoto, I. Kifune, Use of alumina–magnesia castables in steel ladle side wall, Taikabutsu Overseas 17 (3) (1997) 39–44.
[10] (a) S. Mukhopadhyay, et al., Influence of gel-derieved nanocrystalline spinel in a high aluminal castable, Ceram. Int. 31 (2) (2005) 333–347;
(b) S. Mukhopadhyay, et al., Influence of gel-derieved nanocrystalline spinel in a high aluminal castable, Ceram. Int. 33 (2) (2007) 175–186;
(c) S. Mukhopadhyay, P.K. DasPoddar, Effect of preformed and in situ spinels on microstructure and properties of a low cement castable, Ceram. Int. 30 (3) (2004) 369–380.
[11] A. Banerjee, S. Das, S. Misra, S. Mukhopadhyay, Structural analysis on spinel ($MgAl_2O_4$) for application in spinel bonded castables, Ceram. Int. 35 (2009) 381–390.
[12] M. Fuhrer, A. Hey, W.E. Lee, Microstructural evolution in self-forming spinel/calcium aluminate bonded castable refractories, J. Eur. Ceram. Soc. 18 (1998) 813–820.
[13] CRC Press, LLC, Mechanochemistry,, in: H. Masuda, K. Higashitani, H. Yoshida (Eds.), 3rd edition, Powder Technology Handbook, Taylor and Francis, USA, 2006, p. 242.
[14] A.C.D. Chakladar, D. Sarkar and R. Wallin, Development of slag-resistant refractories, in: R.E. Fisher ed. Ceramic Transactions, vol. 4, Advances in Refractories Technology, American Ceramic Society (1989), Ohio, pp. 489–505.
[15] Corrosion of Refractories, C.A. Schacht, D.A. Browson (Eds.), Refractories Handbook, Marcel Dekker Inc., New York, 2004, pp. 75.
[16] I. Ganesh, S. Bhattacharjee, B.P. Saha, R. Johnson, K. Rajeswari, R. Sengupta, M.V. Ramana Rao, Y.R. Mahajan, An efficient $MgAl_2O_4$ spinel additive for improved slag erosion and penetration resistance of high-Al_2O_3 and MgO–C refractories, Ceram. Int. 28 (2002) 245–253.
[17] H. Sarpoolaky, S. Zhang, W.E. Lee, Corrosion of high alumina and near stoichiometric spinels in iron-containing silicate slags, J. Eur. Ceram. Soc. 23 (2) (2003) 293–300.
[18] Y.C. Ko, Role of spinel composition in the slag resistance of Al_2O_3–spinel and Al_2O_3–MgO castables, Ceram. Int. 28 (7) (2002) 805–810.
[19] M.K. Cho, G.G. Hong, S.K. Lee, Corrosion of spinel clinker by CaO–Al_2O_3–SiO_2 ladle slag, J. Eur. Ceram. Soc 22 (11) (2002) 1783–1790.
[20] A. Molin, J. Molin, J. Podworny, Corrosion mechanism of spinel forming and spinel containing refractory castables in lab and plant condition, in: Proceedings of the 9th UNITECR-2005, November 8–11, Orlando, FL, USA, 2005.
[21] R. Riedel (Ed.), Handbook of Ceramic Hard Materials, vol. 1, Wiley–VCH, 2000, p. 140.
[22] S. Harrington, D.-M. Zhu, A. Thirunavukkarasu, A. Misra, Atomic force microscopy study of silica nanopowder compacts, J. Mater. Sci. 34 (1999) 2075–2079.
[23] D.P.H. Hasselman, Unified theory of thermal shock fracture initiation and crack propagation in brittle ceramics, J. Am. Ceram. Soc. 52 (1969) 600–604.
[24] G. Oprea, G. Ye, T. Troczynski, Sintering studies on binding systems for spinel bonded castables, in: Proceedings of the 9th UNITECR-2005, November 8–11, Orlando, FL, USA, 2005.
[25] (a) X.-H. Wang, I.-W. Chen, Sintering of nanoceramics, in: Y. Gogotsi (Ed.), Nanomaterials Handbook, CRC Press, Taylor and Francis Gr., USA, 2006;
(b) J. Li, Y. Ye, L. Shen, J. Chen, H. Zhou, Densification and grain growth during pressureless sintering of TiO_2 nanoceramics, Mater. Sci. Eng. A 390 (1–2) (2005) 265–270.
[26] Z.X. Yang, et al., Effect of spinel formation in Al_2O_3–MgO refractory castables, in: Proceedings of the 9th UNITECR-2005, November 8–11, Orlando, FL, USA, 2005.
[27] M. Rigaud, C. Xing, V. Kovac, Volume stability of spinel-bonded magnesia castables, Euroceramics V, Key Eng. Mater. 132–136 (1997) 1818–1820.